Journal of
Mechanics of
Materials and Structures

A NEW MODEL TO PREDICT THE BEHAVIOR AT THE
INTERFACES OF MULTILAYER STRUCTURES

M. Karama, K. S. Afaq and S. Mistou

A NEW MODEL TO PREDICT THE BEHAVIOR AT THE INTERFACES OF MULTILAYER STRUCTURES

M. KARAMA, K. S. AFAQ AND S. MISTOU

One of the current problems connected with multilayer composite structures concerns the analysis of the distribution of the stresses around peculiarities (free edge and loaded edge) and at the interfaces of each layer. This work presents a new shear stress function in the form of the exponential function to predict the mechanical behavior of multilayered laminated composite structures. As a case study, the mechanical behavior of a laminated composite beam (90°/0°/0°/90°) is examined. The results are compared with the Touratier model *sine* and the two-dimensional finite element method studied. Results show that this new model is more precise than older ones when compared with results obtained by finite element analysis. To introduce continuity on the interfaces of each layer, the new exponential model is used with Ossadzow kinematics. The equilibrium equations and natural boundary conditions are derived from the principle of virtual power.

Notations

h beam thickness or height

h_1 transverse shear function

H Heaviside step function

L beam length

m layer number

P^* virtual power

u_α membrane displacement

$\ddot{U}$ differentiation with respect to time $= \partial^2 U/\partial t^2$

$U_{1,1}$ differentiation with respect to $x_1 = \partial U_1/\partial x_1$

U^* virtual displacements

U^{*^T} the vector of virtual displacements transposed

w transverse displacement

$\bar{\bar{D}}^*$ virtual tensor of the deformations

$\vec{f}$ vector forces of volume

$\vec{F}$ vector forces of surface

Greek letters

γ, ϕ transverse shear rotation

ε strain

σ stress

$\bar{\bar{\sigma}}$ stress tensor

1. Introduction

One of the major challenges in computational structural mechanics is the development of the advanced models and numerical techniques in order to provide efficient tools exhibiting good interior and edge solutions.

In this paper we are introducing an *exponential function* as a shear stress function; the exponential functions are found to be much richer than trigonometric sine and cosine functions in their development series. According to the definition of the transverse shear stress function, the existing laminated composite beam is divided into two broad categories: the global approximation models and the discrete layer approximation models. The equivalent single-layer laminate theories are those in which a heterogeneous laminated plate is treated as a statically equivalent single layer having a complex constitutive behavior, enabling the three-dimensional continuum problem to be considered as a two-dimensional one.

The equivalent single layer models are:

- The [Kirchhoff 1850; Love 1934] theory (or classical theory) in which deformation due to transverse shear is neglected, implies that the normal to the mid-plane remains straight and normal at mid-surface after deformation. This theory can be used for thin beams.

- The [Reissner 1945; Mindlin 1951] theory (or first-order theory). The first-order deformation theory increases the kinematics of the classical laminated plate theory by including a gross transverse shear deformation in its kinematical assumption. That the transverse shear strain remains constant with respect to the thickness coordinate implies that the normal to the mid plane remains straight but not normal at mid-surface after deformation due to the shear effect. The first-order theory requires shear correction factors, which are difficult to determine for arbitrary laminated composite plates.

- The higher-order models are based on the hypothesis of nonlinear stress variation through thickness [Reddy 1984; Touratier 1991]. These models are able to represent the section warping in the deformed configuration.

However, these theories do not satisfy the continuity conditions of transverse shear stress at layer interfaces. Although the discrete layer approximation theories are accurate, they are rather complex for problem solving because the order of their governing equations depends on the number of layers.

DiSciuva [1987; 1993] and Turatier [1991; 1992] proposed simplified discrete layer models with only five variational unknowns (two membrane displacements, a transverse displacement and two rotations), making it possible for the section in the deformed configuration to be represented by warping in the [Touratier 1992] model. Nevertheless, in these two cases compatibility conditions, both for layer interfaces and boundaries, cannot be satisfied. From Touratier's work, [Beakou 1991] and [Idlbi 1995]

proposed, respectively, shell and plate models which satisfy both the stress continuity at the interfaces and the zero stress conditions at the free boundaries.

Finally, He [1994] introduced the Heaviside step function which enables automatic satisfaction of the displacement continuity at interfaces between different layers. The new discrete layer model presented comes from the work of [Di Sciuva 1993; He 1994; Ossadzow et al. 1995]. The displacement field is assumed to be of the form:

$$U_1(x_1, x_3, t) = u_1^0(x_1, t) - x_3 w_{,1}(x_1, t) + h_1(x_3)\phi_1(x_1, t),$$
$$U_2 = 0,$$
$$U_3(x_1, t) = w(x_1, t), \tag{1}$$

with the transverse shear function

$$h_1(x_3) = g(x_3) + \sum_{m=1}^{N-1} \lambda_1^{(m)}\left(-\tfrac{1}{2}x_3 + \tfrac{1}{2}f(x_3) + (x_3 - x_3^{(m)})H(x_3 - x_3^{(m)})\right),$$

where $H(x_3 - x_3^{(m)})$ is the Heaviside Step function defined as

$$H(x_3 - x_3^{(m)}) = \begin{cases} 1 & \text{for } x_3 \geq x_3^{(m)}, \\ 0 & \text{for } x_3 < x_3^{(m)}, \end{cases} \tag{2}$$

$f(x_3)$ is the shear refinement function, $g(x_3)$ is the membrane refinement function, and $\lambda_I^{(m)}$ are continuity coefficients.

1.1. *New multilayered laminated composite structures model ("KAM").* In this work a new multilayered laminated composite structure model representing the shear and membrane functions using exponential functions as follows:

$$f(z) = ze^{-2(z/h)^2}, \qquad g(z) = -ze^{-2(z/h)^2}, \tag{3}$$

for a multilayered beam of uniform thickness h defined on the domain Ω, which refers to the coordinate system $R = (0/x_1, x_2, x_3 = z)$, with z being normal at plate mid-surface Σ, and Γ as the boundary of Ω. Then, the domain Ω is such that

$$\Omega = \left\{\Sigma \times \left(-\frac{h}{2}, \frac{h}{2}\right) \middle| -\frac{h}{2} \leq z \leq \frac{h}{2M(x_1, x_2, z)} \in \Omega, \, M_o(x_1, x_2, 0) \in \Sigma, \, \phi \gg \text{Max}(z)\right\} \subset R^3,$$

where ϕ is the diameter of the Ω and the closed domain $\bar{\Omega}$ is set by

$$\bar{\Omega} = \left\{\Omega \cup \Gamma / \Gamma = \Gamma_{\text{edge}} \cup \Gamma_{z=\pm h/2}\right\}.$$

From the beginning our objective was clear, namely, to find the transverse shear stress function $f(z)$ that gives the mechanical behavior of the composite laminated structures as close as possible to that of the exact three-dimensional solution [Pagano 1970] or the finite element analysis in two dimensions (stress, strain plane), and with better representation of the transverse shear stress in the thickness of the laminated structure. Several different higher-order polynomial and trigonometric functions already had been tried:

- [Ambartsumian 1958]: $f(z) = \frac{z}{2}\left(\frac{h^2}{4} - \frac{z^2}{3}\right)$,

- [Kaczkowski 1968; Panc 1975; Reissner 1975]: $f(z) = \frac{5}{4}z\left(1 - \frac{4z^2}{3h^2}\right)$,

- [Levinson 1980; Murthy 1981; Reddy 1984]: $f(z) = z\left(1 - \frac{4z^2}{3h^2}\right)$,

- [Touratier 1991]: $f(z) = \frac{h}{\pi}\sin\left(\frac{\pi z}{h}\right)$.

We began with an exponential function, since that function has all even and odd powers in its expansion (see the present model) unlike sine functions (see the Touratier model), which have only odd powers. Then an exponential function is much richer than a sine function. If we take a look at the expansions of different transverse shear stress functions,

- [Reddy 1984]: $f(z) = z\left(1 - \frac{4z^2}{3h^2}\right) = z - 1.33\frac{z^3}{h^2}$,

- [Touratier 1991]: $f(z) = \frac{h}{\pi}\sin\left(\frac{\pi z}{h}\right) = z - 1.645\frac{z^3}{h^2} + 0.812\frac{z^5}{h^4} - 0.191\frac{z^7}{h^6} + 0.0261\frac{z^9}{h^8}$,

- Present Model: $f(z) = ze^{-2(z/h)^2} = z - 2\frac{z^3}{h^2} + 2\frac{z^5}{h^4} - 1.333\frac{z^7}{h^6} + 0.666\frac{z^9}{h^8}$,

it is clear from expansions of the transverse shear stress functions that the coefficient of successive terms in sine functions decreases more rapidly than the present exponential function. These expansions are the main influences for the different mechanical behaviors of laminated structures.

For the transverse shear stress behavior, it is very important that the first derivative of the transverse shear stress function provide a parabolic response in the thickness direction of the laminate and that it satisfy the boundary conditions.

2. Governing equations

From the virtual power principle, the equations of motion and the natural boundary conditions can be obtained. The calculations are made in small perturbations. According to the principle of virtual power,

$$P^*_{(a)} = P^*_{(i)} + P^*_{(e)}, \tag{4}$$

where $P^*_{(a)}$, $P^*_{(i)}$, $P^*_{(e)}$ correspond to virtual power of the acceleration quantities, virtual power of internal work and the virtual power of external loading.

The virtual power of the acceleration quantities is:

$$P^*_{(a)} = \int_{\Omega} \rho U^{*T} \ddot{U} d\Omega, \tag{5}$$

where U^* and U^{*T} are virtual displacements and the vector of virtual displacements transposed.

Assuming

$$I_w = \int_{-h/2}^{h/2} \rho \, dx_3, \qquad I_{uw'} = -\int_{-h/2}^{h/2} \rho x_3 \, dx_3,$$

$$I_{w'} = \int_{-h/2}^{h/2} \rho x_3^2 \, dx_3, \qquad I_{u\omega} = \int_{-h/2}^{h/2} \rho h_1(x_3) \, dx_3, \tag{6}$$

$$I_{\omega} = \int_{-h/2}^{h/2} \rho h_1^2(x_3) \, dx_3, \qquad I_{\omega w'} = -\int_{-h/2}^{h/2} \rho x_3 h_1(x_3) \, dx_3,$$

Equation (5) becomes

$$P^*_{(a)} = \int_0^L \left(\Gamma^{(u)} u_1^{0*} + \Gamma^{(w)} w^* + \Gamma^{(\phi)} \phi_1^* \right) dx_1 + \bar{\Gamma}^{(w)} w^*, \tag{7}$$

where,

$$\Gamma^{(u)} = I_w \ddot{u}_1^o + I_{uw'} \ddot{w}_{,1} + I_{u\omega} \ddot{\phi}_1, \qquad \Gamma^{(w)} = -I_{uw'} \ddot{u}_{1,1}^o + I_w \ddot{w} - I_{w'} \ddot{w}_{,11} - I_{\omega w'} \ddot{\phi}_{1,1},$$

$$\Gamma^{(\phi)} = I_{u\omega} \ddot{u}_1^o + I_{\omega w'} \ddot{w}_{,1} + I_\omega \ddot{\phi}_1, \qquad \bar{\Gamma}^{(w)} = I_{uw'} \ddot{u}_1^o + I_{w'} \ddot{w}_{,1} + I_{\omega w'} \ddot{\phi}_1.$$

See Section A for details.

Now the virtual power of internal work is

$$P^*_{(i)} = \int_\Omega \overline{\overline{D}}^{*T} : \overline{\overline{\sigma}} d\Omega, \tag{8}$$

where $\overline{\overline{D}}^*$ is the virtual tensor of deformation and $\overline{\overline{\sigma}}$ is the tensor of the constraints.

Since

$$\overline{\overline{D}}^* = \begin{vmatrix} D^*{}_{11} & D^*{}_{12} & D^*{}_{13} \\ D^*{}_{21} & D^*{}_{22} & D^*{}_{23} \\ D^*{}_{31} & D^*{}_{32} & D^*{}_{33} \end{vmatrix}, \qquad \overline{\overline{\sigma}} = \begin{vmatrix} \sigma_{11} & \sigma_{12} & \sigma_{13} \\ \sigma_{21} & \sigma_{22} & \sigma_{23} \\ \sigma_{31} & \sigma_{32} & \sigma_{33} \end{vmatrix},$$

in two dimensions

$$\overline{\overline{D}}^* : \overline{\overline{\sigma}} = D^*_{11} \sigma_{11} + 2 D^*_{13} \sigma_{13}. \tag{9}$$

Resultant stresses $N_{\alpha\beta}$, $M_{\alpha\beta}$ and $P_{\alpha\beta}$ are defined as

$$N_{11} = \int_{-h/2}^{h/2} \sigma_{11} dx_3, \qquad M_{11} = \int_{-h/2}^{h/2} x_3 \sigma_{11} dx_3,$$

$$P_{11} = \int_{-h/2}^{h/2} h_1(x_3) \sigma_{11} dx_3, \qquad P_{13} = \int_{-h/2}^{h/2} h_{1,3}(x_3) \sigma_{13} dx_3, \tag{10}$$

so Equation (8) becomes

$$P^*_{(i)} = \int_0^L \left(N_{11,1} u_1^{0*} + M_{11,11} w^* + (P_{11,1} - P_{13}) \phi_1^* \right) dx_1 - N_{11} u_1^{0*} - M_{11,1} w^* + M_{11} w_{,1}^* - P_{11} \phi_1^*. \tag{11}$$

See Section B for details.

Now the virtual power of external loading is

$$P^*_{(e)} = \int_\Omega U^{*T} . \vec{f} \, d\Omega + \int_\Gamma U^{*T} \vec{F} \, d\Gamma. \tag{12}$$

Here

$$U^{*T} = \begin{bmatrix} U_1^* & 0 & U_3^* \end{bmatrix}, \qquad \vec{f} = \begin{bmatrix} f_1 \\ f_2 \\ f_3 \end{bmatrix}, \qquad \vec{F} = \begin{bmatrix} F_1 \\ F_2 \\ F_3 \end{bmatrix},$$

where $\vec{f}$ and $\vec{F}$ are the vector forces of volume and surface, respectively, with

$$U_1^* = u_1^{0*} - x_3 w_{,1}^* + h_1(x_3)\phi_1^*,$$
$$U_2^* = 0,$$
$$U_3^* = w^*.$$

We define

$$\bar{n}_i = \int_{-h/2}^{h/2} f_i dx_3, \qquad \bar{N}_i = \int_{-h/2}^{h/2} F_i dx_3,$$
$$\bar{m}_i = \int_{-h/2}^{h/2} x_3 f_i dx_3, \qquad \bar{M}_i = \int_{-h/2}^{h/2} x_3 F_i dx_3, \qquad (13)$$
$$\bar{p}_i = \int_{-h/2}^{h/2} h_1(x_3) f_i dx_3, \qquad \bar{P}_i = \int_{-h/2}^{h/2} h_1(x_3) F_i dx_3,$$

so Equation (12) becomes

$$P_{(e)}^* = \int_0^L \left(\bar{n}_1 u_1^{0*} + (\bar{n}_3 + \bar{m}_{1,1})w^* + \bar{p}_1\phi_1^*\right)dx_1 + \bar{N}_1 u_1^{0*}(\bar{N}_3 - \bar{m}_1)w^* - \bar{M}_1 w_{,1}^* + \bar{P}_1\phi_1^*. \qquad (14)$$

See Section C for details.

Now, by Equations (4), (7), (11) and (14), governing equations and natural boundary conditions for all u_1^{0*}, w^*, ϕ_1^* we have

$$\Gamma^{(u)} = N_{11,1} + \bar{n}_1,$$
$$\Gamma^{(w)} = M_{11,11} + (\bar{n}_3 + \bar{m}_{1,1}), \qquad (15)$$
$$\Gamma^{(\phi)} = P_{11,1} - P_{13} + \bar{p}_1.$$

And natural boundary conditions for all u_1^{0*}, w^*, ϕ_1^*, $w_{,1}^*$ are

$$\bar{\Gamma}^{(w)} = -M_{11,1} + \left(\bar{N}_3 - \bar{m}_1\right), \qquad 0 = -N_{11} + \bar{N}_1 = -P_{11} + \bar{P}_1 = M_{11} - \bar{M}_1. \qquad (16)$$

The three-dimensional orthotropic constitutive law is

$$\begin{Bmatrix} \sigma_{11} \\ \sigma_{22} \\ \sigma_{33} \\ \sigma_{23} \\ \sigma_{13} \\ \sigma_{12} \end{Bmatrix} = \begin{bmatrix} C_{11} & C_{12} & C_{13} & 0 & 0 & 0 \\ C_{12} & C_{22} & C_{23} & 0 & 0 & 0 \\ C_{13} & C_{23} & C_{33} & 0 & 0 & 0 \\ 0 & 0 & 0 & C_{44} & 0 & 0 \\ 0 & 0 & 0 & 0 & C_{55} & 0 \\ 0 & 0 & 0 & 0 & 0 & C_{66} \end{bmatrix} \begin{Bmatrix} \varepsilon_{11} \\ \varepsilon_{22} \\ \varepsilon_{33} \\ 2\varepsilon_{23} \\ 2\varepsilon_{13} \\ 2\varepsilon_{12} \end{Bmatrix}. \qquad (17)$$

The dimension according to x_2 is supposed to be equal to the unit and the effects of the σ_{33} are neglected, so orthotropic law (17) becomes

$$\begin{Bmatrix} \sigma_{11} \\ \sigma_{13} \end{Bmatrix} = \begin{bmatrix} C_{11}' & 0 \\ 0 & C_{55} \end{bmatrix} \begin{Bmatrix} \varepsilon_{11} \\ 2\varepsilon_{13} \end{Bmatrix}, \qquad (18)$$

with $\varepsilon_{11} = U_{1,1} = u_{1,1}^{0*} - x_3 w_{,11} + h_1 \phi_{1,1}$, $2\varepsilon_{31} = h_{1,3}\phi_1$, and

$$C_{11}' = \frac{C_{11}C_{33} - C_{13}^2}{C_{33}}.$$

Now, the generalized constitutive law is

$$\begin{bmatrix} N_{11} \\ M_{11} \\ P_{11} \\ P_{13} \end{bmatrix} = \begin{bmatrix} A_{11} & B_{11} & \tilde{K} & 0 \\ B_{11} & D_{11} & \tilde{T} & 0 \\ \tilde{K} & \tilde{T} & \tilde{S} & 0 \\ 0 & 0 & 0 & \tilde{Y} \end{bmatrix} \begin{bmatrix} u_{1,1}^{0*} \\ -w_{,11} \\ \phi_{1,1} \\ \phi_1 \end{bmatrix}.$$

So, the governing equations (15) become

$$\Gamma^{(u)} = A_{11}u_{1,11}^{0*} - B_{11}w_{,111} + \tilde{K}\phi_{1,11} + \bar{n}_1,$$

$$\Gamma^{(w)} = B_{11}u_{1,111}^{0*} - D_{11}w_{,1111} + \tilde{T}\phi_{1,111} + \bar{n}_3 + \overline{m}_{1,1}, \tag{19}$$

$$\Gamma^{(\phi)} = \tilde{K}u_{1,11}^{0*} - \tilde{T}w_{,111} + \tilde{S}\phi_{1,11} - \tilde{Y}\phi_1 + \overline{p}_1.$$

Then the natural boundary conditions (16) become

$$0 = A_{11}u_{1,1}^{0*} - B_{11}w_{,11} - \tilde{K}\phi_{1,1} + \bar{N}_1,$$

$$\bar{\Gamma}^{(w)} = -B_{11}u_{1,11}^{0*} + D_{11}w_{,111} - \tilde{T}\phi_{1,11} + \bar{N}_3 - \bar{m}_1,$$

$$0 = -\tilde{K}u_{1,1}^{0*} + \tilde{T}w_{,11} - \tilde{S}\phi_{1,1} + \overline{P}_1, \tag{20}$$

$$0 = -B_{11}u_{1,1}^{0*} - D_{11}w_{,11} + \tilde{T}\phi_{1,1} - \bar{M}_1.$$

2.1. *Continuity coefficients* (λ). To find out the value of the continuity coefficients, the conditions of the continuity of the transverse shear stress between each layer interface were used (see Figure 1):

$$\sigma_{13}^{(m)}(x_3 = x_3^{(m)}) = \sigma_{13}^{(m+1)}(x_3 = x_3^{(m)}).$$

Interface of layer 1 and layer 2 also gives

$$\sigma_{13}^{(1)}(x_3 = x_3^{(1)}) = \sigma_{13}^{(2)}(x_3 = x_3^{(1)}),$$

and

$$Q_{55}^1\phi(x_1)\left[g'(x_3^{(1)}) + \tfrac{1}{2}\left(\lambda_1^{(1)} + \lambda_1^{(2)} + \lambda_1^{(3)}\right)\left(-1 + f'(x_3^{(1)})\right)\right]$$
$$= Q_{55}^2\phi(x_1)\left[g'(x_3^{(1)}) + \tfrac{1}{2}\left(\lambda_1^{(1)} + \lambda_1^{(2)} + \lambda_1^{(3)}\right)\left(-1 + f'(x_3^{(1)})\right) + \lambda_1^{(1)}\right]. \tag{21}$$

Interface of layer 2 and layer 3 gives

$$\sigma_{13}^{(2)}(x_3 = x_3^{(2)}) = \sigma_{13}^{(3)}(x_3 = x_3^{(2)}).$$
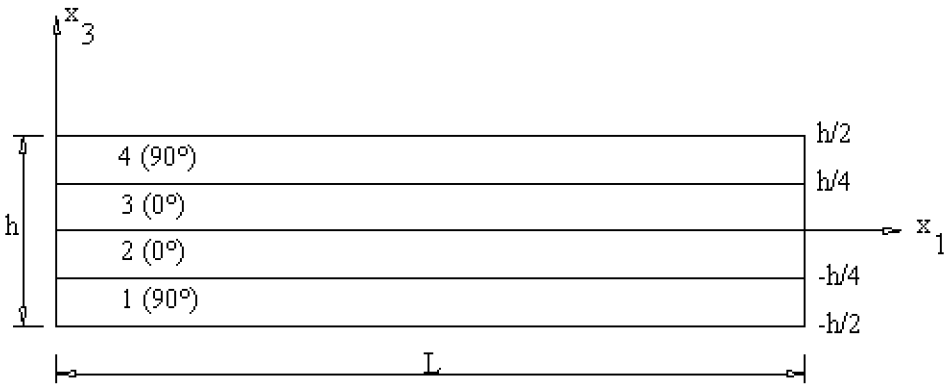
Figure 1. Side view of a laminated composite beam $(90°/0°/0°/90°)$.

Since Q_{55} of the second and third layer are equal (Figure 1), we get

$$Q_{55}^2 \phi(x_1)\left[g'(x_3^{(2)}) + \tfrac{1}{2}(\lambda_1^{(1)} + \lambda_1^{(2)} + \lambda_1^{(3)})(-1 + f'(x_3^{(2)})) + \lambda_1^{(1)}\right]$$
$$= Q_{55}^3 \phi(x_1)\left[g'(x_3^{(2)}) + \tfrac{1}{2}(\lambda_1^{(1)} + \lambda_1^{(2)} + \lambda_1^{(3)})(-1 + f'(x_3^{(2)})) + \lambda_1^{(1)} + \lambda_1^{(2)}\right]. \quad (22)$$

Now, by Equations (21) and (22),

$$\lambda_1^{(1)} = \lambda_1^{(1)} + \lambda_1^{(2)},$$
$$\lambda_1^{(2)} = 0. \quad (23)$$

This shows that if the mechanical characteristics of the two consecutive layers are the same (Figure 1), the coefficient of the continuity will be zero $(\lambda^{(2)} = 0)$.

Interface of layer 3 and layer 4 gives

$$\sigma_{13}^{(3)}(x_3 = x_3^{(3)}) = \sigma_{13}^{(4)}(x_3 = x_3^{(3)})$$

and

$$Q_{55}^3 \phi(x_1)\left[g'(x_3^{(3)}) + \tfrac{1}{2}(\lambda_1^{(1)} + \lambda_1^{(2)} + \lambda_1^{(3)})(-1 + f'(x_3^{(3)})) + \lambda_1^{(1)} + \lambda_1^{(2)}\right] =$$
$$Q_{55}^4 \phi(x_1)\left[g'(x_3^{(3)}) + \tfrac{1}{2}(\lambda_1^{(1)} + \lambda_1^{(2)} + \lambda_1^{(3)})(-1 + f'(x_3^{(3)})) + \lambda_1^{(1)} + \lambda_1^{(2)} + \lambda_1^{(3)}\right], \quad (24)$$

where

$$f'(x_3^{(1)} = -h/4) = f'(x_3^{(3)} = h/4),$$
$$g'(x_3^{(1)} = -h/4) = g'(x_3^{(3)} = h/4).$$

So, using Equations (22)–(24), we obtain

$$Q_{55}^1 \phi(x_1) \left[g'(x_3^{(3)}) + \tfrac{1}{2}(\lambda_1^{(1)} + \lambda_1^{(2)} + \lambda_1^{(3)})(-1 + f'(x_3^{(3)})) \right]$$
$$= Q_{55}^4 \phi(x_1) \left[g'(x_3^{(3)}) + \tfrac{1}{2}(\lambda_1^{(1)} + \lambda_1^{(2)} + \lambda_1^{(3)})(-1 + f'(x_3^{(3)})) + \lambda_1^{(1)} + \lambda_1^{(3)} \right] \quad (25)$$

and

$$0 = \lambda_1^{(1)} + \lambda_1^{(3)} \quad \longrightarrow \quad \lambda_1^{(1)} = -\lambda_1^{(3)}. \quad (26)$$

So, by Equations (23) and (25), Equation (21) becomes

$$Q_{55}^1(g'(x_3^{(1)})) = Q_{55}^2(g'(x_3^{(1)}) + \lambda_1^{(1)}), \qquad \lambda_1^{(1)} = \frac{(Q_{55}^1 - Q_{55}^2)g'(x_3^{(1)})}{Q_{55}^2},$$
$$\lambda_1^{(3)} = \frac{(Q_{55}^2 - Q_{55}^1)g'(x_3^{(1)})}{Q_{55}^2}. \quad (27)$$

2.2. *Finite element analysis.* Since no exact three-dimensional solution exists for the considered case study, ABAQUS (finite element analysis software) is used to show the efficiency of the present model. In this paper, finite element results are taken as a reference for the comparison of different models of laminated composite structures, done by Karama et al. [1998]. The three-dimensional approximation of the behavior is carried out by element type "CPS8" (quadrilateral element of eight nodes, 16 dof per element). To validate the finite element results, it is first necessary to find out the convergence of laminate meshing. So, for the given problem, in static and dynamic, the convergence is obtained with 1680 elements, including 24 elements of thickness.

3. Some evaluations of the present model

3.1. *Bending analysis.* The static bending analysis is studied, so the virtual power of acceleration quantities is canceled. Three different bending analyses have been developed for three different specific boundary conditions. For the simply supported conditions, the unknown variables are deduced directly by the equation of motions. For clamped conditions, kinematical boundary conditions are used and, finally, in a free edge case, natural boundary conditions are employed.

The beam studied has a length of $L = 6.35 \, \text{m}$, a unitary width, and a thickness $h = 2.794 \, \text{m}$ in the thick case and $h = 0.2794 \, \text{m}$ in the thin case. The beam possesses four layers of the same thickness at $90°/0°/0°/90°$. The material used for the four layers is boron epoxy. The mechanical properties of the $0°$ layer are as follows [Widera and Logan 1980]:

$$E_{11} = 241.5 \, \text{GPa}, \qquad E_{22} = E_{33} = 18.89 \, \text{GPa}, \qquad G_{12} = G_{13} = 5.18 \, \text{GPa}, \qquad \rho = 2015 \, \text{kg/m}^3,$$
$$G_{23} = 3.45 \, \text{GPa}, \qquad v_{23} = 0.25, \qquad\qquad v_{12} = v_{13} = 0.24,$$

The continuity coefficients from Equations (23), (26)–(27) are evaluated as

$$\lambda_1^{(1)} = -\lambda_1^{(3)} = 0.2210501411, \qquad \lambda_1^{(2)} = 0.$$

3.2. *Bending of a simply supported beam under distributed sinusoidal load.* The surface and volume force components are canceled except for

$$\bar{n}_3 = \int_0^h f_3 dx_3 = q = q_o \sin\left(\frac{\pi x_1}{L}\right).$$

For the simply supported boundary conditions, the Levy solution is used, which is defined as

$$u_1^o = u_o \cos\left(\frac{\pi x_1}{L}\right), \qquad w = w_o \sin\left(\frac{\pi x_1}{L}\right), \qquad \phi_1 = \phi_o \cos\left(\frac{\pi x_1}{L}\right).$$

Now, the governing equations (19) with $P_{(a)}^* = 0$ become

$$0 = A_{11} u_{1,11}^{0*} - B_{11} w_{,111} + \tilde{K}\phi_{1,11},$$

$$0 = B_{11} u_{1,111}^{0*} - D_{11} w_{,1111} + \tilde{T}\phi_{1,111} + q_o \sin\left(\frac{\pi x_1}{L}\right),$$

$$0 = \tilde{K} u_{1,11}^{0*} - \tilde{T} w_{,111} + \tilde{S}\phi_{1,11} - \tilde{Y}\phi_1.$$

For the Levy solution, the governing equations become

$$0 = -A_{11}\alpha^2 u_o \cos\alpha x_1 + B_{11}\alpha^3 w_o \cos\alpha x_1 - \tilde{K}\alpha^2\phi_o \cos\alpha x_1,$$

$$0 = B_{11}\alpha^3 u_o \sin\alpha x_1 - D_{11}\alpha^4 w_o \sin\alpha x_1 + \tilde{T}\alpha^3\phi_o \sin\alpha x_1 + q_o \sin\alpha x_1,$$

$$0 = -\tilde{K}\alpha^2 u_o \cos\alpha x_1 + \tilde{T}\alpha^3 w_o \cos\alpha x_1 - \tilde{S}\alpha^2\phi_o \cos\alpha x_1 - \tilde{Y}\phi_o \cos\alpha x_1,$$

with $\alpha = \pi/L$. In matrix form,

$$\begin{bmatrix} -\alpha^2 A_{11} & \alpha^3 B_{11} & -\alpha^2 \tilde{K} \\ \alpha^3 B_{11} & -\alpha^4 D_{11} & \alpha^3 \tilde{T} \\ -\alpha^2 \tilde{K} & \alpha^3 \tilde{T} & -\alpha^2 \tilde{S} - \tilde{Y} \end{bmatrix} \begin{pmatrix} u_o \\ w_o \\ \phi_o \end{pmatrix} = \begin{pmatrix} 0 \\ -q_o \\ 0 \end{pmatrix}.$$

Also, the displacement (1), becomes

$$U_1(x_1, x_3) = (u_o - x_3 w_o \alpha + h_1(x_3)\phi_o) \cos(\alpha x_1),$$

$$U_2 = 0,$$

$$U_3 = w_o \sin(\alpha x_1),$$

and by relation (18), the stresses are

$$\sigma_{11}(x_1, x_3) = -\alpha C_{11}'(u_o - \alpha x_3 w_o + h_1\phi_o) \sin(\alpha x_1),$$

$$\sigma_{13}(x_1, x_3) = C_{55} h_{1,3}\phi_o \cos(\alpha x_1).$$

Integration of the equilibrium equation $\sigma_{13,1} + \sigma_{33,3} = 0$ enables us to calculate the analytical value of σ_{33}, giving

$$\sigma_{33} = \alpha C_{55} h_1(x_3)\phi_o \sin(\alpha x_1).$$

The numerical results obtained ($q_0 = -10^6$ Pa) using the present model are compared with those obtained by the finite element analysis [Karama et al. 1998] and the sine model [Touratier 1991] in Table 1. For this problem, the present model predicts mechanical behavior more accurately than the sine

Model	$U_3(L/2)$	$U_1(h/2)$	$\sigma_{13}(L/4, 0)$ (Interface)	$\sigma_{11}(L/2, -h/4)$ (Interface)	$\sigma_{33}(L/2, h/2)$
	[m]	[m]	[Pa]	[Pa]	[Pa]
Present	6.3701×10^{-4}	2.1196×10^{-4}	-940098.0	8112840.0	-1039990.0
(error)	(4.4%)	(8.3%)	(6.6%)	(3.5%)	(3.9%)
Sine	-6.2794×10^{-4}	2.0180×10^{-4}	-896865.0	8158932.0	-1047274.0
(error)	(2.9%)	(12.7%)	(10.8%)	(4.1%)	(4.6%)
Abaqus	-6.1006×10^{-4}	2.3125×10^{-4}	-1006000.0	7835200.0	-1000900.0

Table 1. Bending of the simply supported thick beam under distributed sinusoidal load.

model when compared to the finite element analysis results, except for the transverse deflection (U_3). Percentage error reduction is more significant in the case of transverse shear stress (σ_{13}) at the interfaces between layers.

The efficiency of this model is shown in Figures 2–5; different stresses and displacements plotted according to the length and thickness of the beam show that, at every point on the beam, the present model is closer to the finite element results then are those of the sine model. Here we can also see the continuity of displacement and transverse shear stress between layer interfaces of the present model.

3.3. *Bending of a clamped free beam under distributed uniform load.* In this case the value of $\bar{n}_3$ is:

$$\bar{n}_3 = \int_{-h/2}^{h/2} f_3 dx_3 = q.$$

Now, the governing equations from the system of Equations (19) takes the form

$$0 = A_{11}u_{1,11}^{0*} - B_{11}w_{,111} + \tilde{K}\phi_{1,11},$$
$$0 = B_{11}u_{1,111}^{0*} - D_{11}w_{,1111} + \tilde{T}\phi_{1,111} + q,$$
$$0 = \tilde{K}u_{1,11}^{0*} - \tilde{T}w_{,111} + \tilde{S}\phi_{1,11} - \tilde{Y}\phi_1.$$

Integrating and simultaneously solving the above equations, gives

$$\phi_1(x_1) = C_1 e^{-Px_1} + C_2 e^{Px_1} - (qx_1 + C_3)\frac{\tilde{T}}{\tilde{Y}D_{11}},$$

$$u_1^o(x_1) = -\frac{\tilde{K}}{A_{11}}\phi_1(x_1) + C_7 x_1 + C_8,$$

$$w(x_1) = \frac{\tilde{T}}{PD_{11}}\left[C_1 e^{-Px_1} + C_2 e^{Px_1} - \left(\tfrac{1}{2}qx_1^2 + C_3 x_1\right)\frac{P}{\tilde{Y}}\right] + \frac{1}{D_{11}}\left(\tfrac{1}{24}qx_1^4 + \tfrac{1}{6}C_3 x_1^3\right) + \tfrac{1}{2}C_4 x_1^2 + C_5 x + C_6,$$

where

$$P = \sqrt{\frac{-\tilde{Y}A_{11}D_{11}}{\tilde{K}^2 D_{11} + \tilde{T}^2 A_{11} - \tilde{S}A_{11}D_{11}}},$$

and $B_{11} = 0$ due to the symmetry at mid-surface. The eight constants C_i are determined by the four natural boundary conditions at the free edge deduced from (20) with $P_{(a)}^* = 0$:

$$0 = A_{11}u_{1,1}^{0*}(L) - \tilde{K}\phi_{1,1}(L), \qquad\qquad 0 = D_{11}w_{,111}(L) - \tilde{T}\phi_{1,11}(L),$$

$$0 = -\tilde{K}u_{1,1}^{0*}(L) + \tilde{T}w_{,11}(L) - \tilde{S}\phi_{1,1}(L), \quad 0 = -D_{11}w_{,11}(L) + \tilde{T}\phi_{1,1}(L).$$
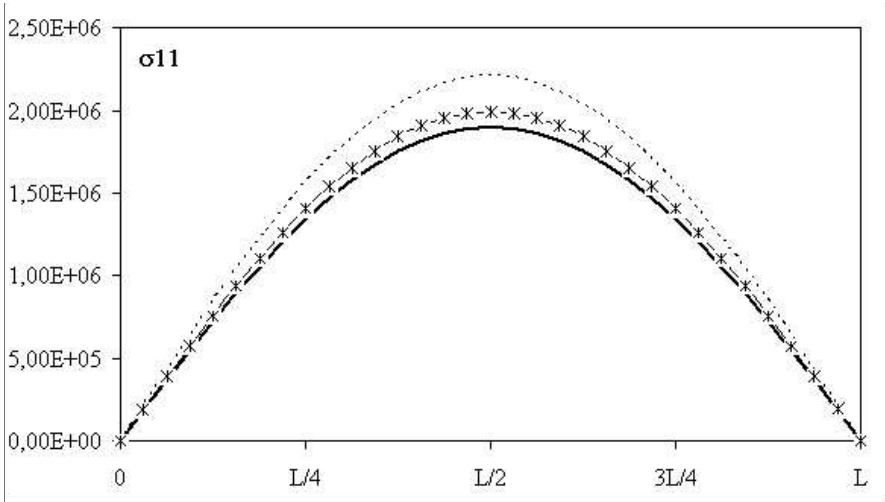
Figure 2. Variation of the stress σ_{11} along the direction x_1 for $x_3 = -\frac{h}{2}$ for Section 3.2. Abaqus (dashed line plot), Sine (solid line), and Present (dashes and crosses).
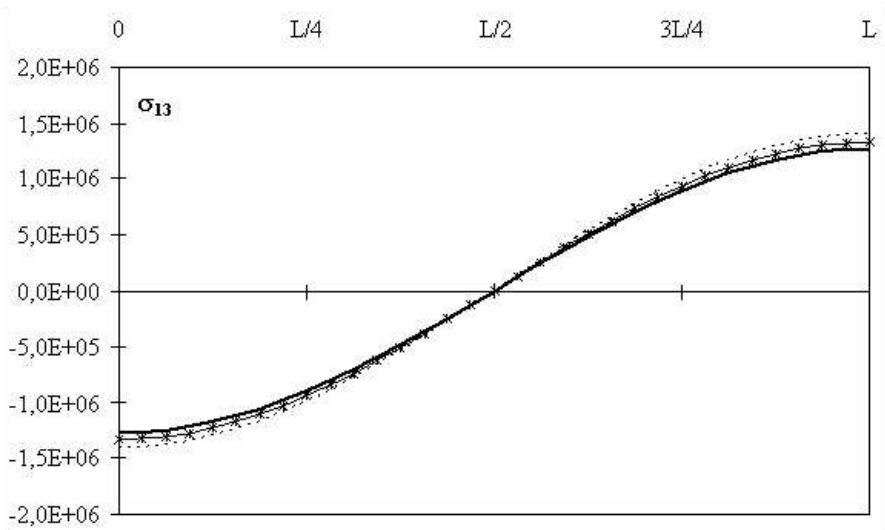
Figure 3. Variation of the transverse shear σ_{13} through the thickness for $x_3 = 0$ (Interface) for Section 3.2. Abaqus (dashed line plot), Sine (solid line), and Present (dashes and crosses).
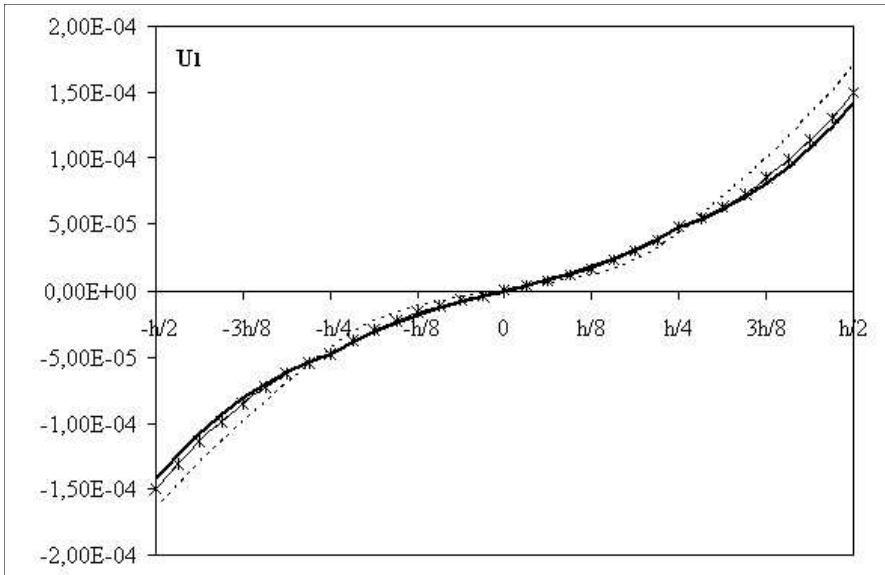
Figure 4. Variation of the displacement U_1 through the thickness for $x_1 = L/4$ for Section 3.2. Abaqus (dashed line plot), Sine (solid line), and Present (dashes and crosses).

The four kinematic boundary conditions at the clamped edge are:

$$u_1^0(0) = 0, \qquad w(0) = 0,$$
$$w_{,1}(0) = 0, \qquad \phi_1(0) = 0.$$

Model	$U_3(L)$	$U_1(L/2, h/2)$	$\sigma_{13}(L/4, 0)$ (Interface)	$\sigma_{11}(L/2, -h/4)$ (Interface)	$\sigma_{33}(L/2, h/2)$
	[m]	[m]	[Pa]	[Pa]	[Pa]
Present	-4.40057×10^{-6}	7.36497×10^{-7}	-3181.03	-9986.18	-1067.10
(error)	(2.6%)	(9.8%)	(-2.3%)	(7.9%)	(-4.3%)
Sine	-4.37885×10^{-6}	7.19163×10^{-7}	-3031.42	-9939.30	-1066.64
(error)	(3.1%)	(11.9%)	(2.5%)	(8.3%)	(-4.3%)
Abaqus	-4.51810×10^{-6}	8.16300×10^{-7}	-3110.00	-10842.00	-1023.00

Table 2. Bending of a clamped/free thick beam under uniformly distributed load.
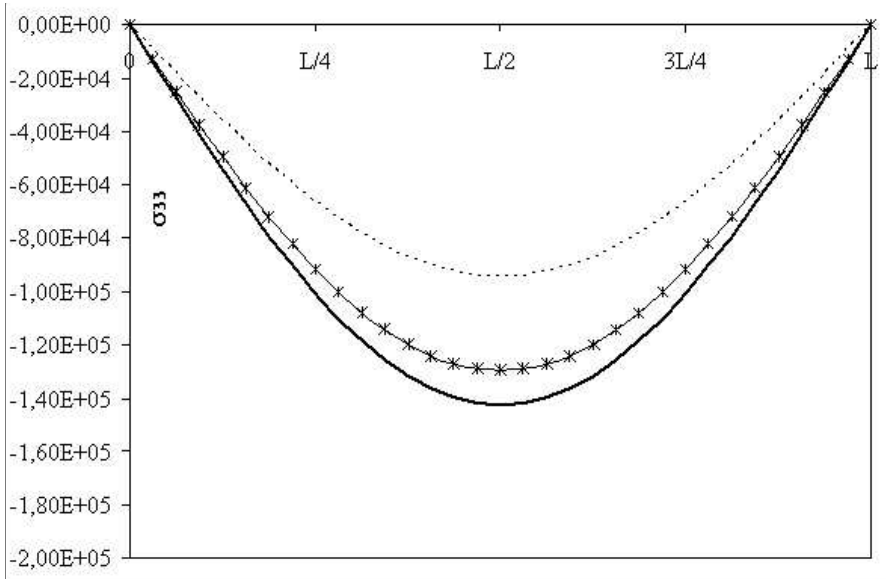
Figure 5. Variation of the stress σ_{33} along the direction x_1 for $x_3 = h/4$ (*Interface*), for Section 3.2. Abaqus (dashed line plot), Sine (solid line), and Present (dashes and crosses).

The numerical results for Table 2 are obtained for a load $q = -1000\,\text{N/m}$ for the same beam as in Section 3.2, except for the load now being uniformly distributed instead of *sinusoidal*, show that the present model still has less percentage of error compared to the sine model. In Figures 6–9, different stresses and displacements are plotted according to the length and thickness of the beam, showing the difference between the present model and sine model as regards the finite element. The present model is in close agreement with the results of Karama et al. [1998].

3.4. *Bending of a clamped free beam under concentrated load.* The load is applied at the free end; in this case the value of $\bar{N}_3$ is:

$$\bar{N}_3 = \int_{-h/2}^{h/2} F_3 dx_3 = q.$$

Now, the governing equation from the system of Equations (19),

$$0 = A_{11}u_{1,11}^{0*} - B_{11}w_{,111} + \tilde{K}\phi_{1,11},$$
$$0 = B_{11}u_{1,111}^{0*} - D_{11}w_{,1111} + \tilde{T}\phi_{1,111},$$
$$0 = \tilde{K}u_{1,11}^{0*} - \tilde{T}w_{,111} + \tilde{S}\phi_{1,11} - \tilde{Y}\phi_1,$$
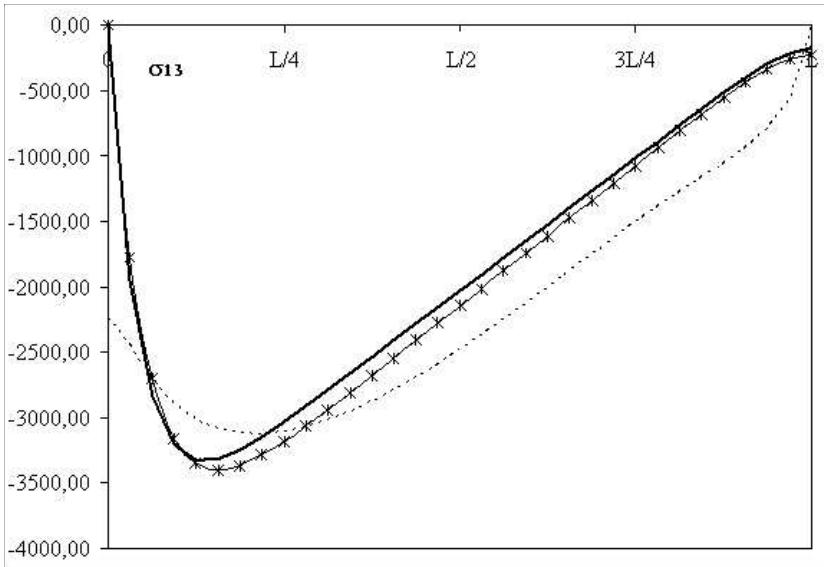
Figure 6. Variation of the stress σ_{13} along the direction x_1 for $x_3 = 0$ (*Interface*) for Section 3.3. Abaqus (dashed line plot), Sine (solid line), and Present (dashes and crosses).

by integration and simultaneous solving of the above equations, gives

$$\phi_1(x_1) = C_1 e^{-Px_1} + C_2 e^{Px_1} - C_3 \frac{\tilde{T}}{\tilde{Y} D_{11}},$$

$$u_1^o(x_1) = -\frac{\tilde{K}}{A_{11}}\phi_1(x_1) + C_7 x_1 + C_8,$$

$$w(x_1) = \frac{\tilde{T}}{PD_{11}}\left[C_1 e^{-Px_1} + C_2 e^{Px_1} - C_3 x_1 \frac{P}{\tilde{Y}}\right] + \frac{C_3}{6D_{11}}x_1^3 + \tfrac{1}{2}C_4 x_1^2 + C_5 x + C_6,$$

where

$$P = \sqrt{\frac{-\tilde{Y}A_{11}D_{11}}{\tilde{K}^2 D_{11} + \tilde{T}^2 A_{11} - \tilde{S}A_{11}D_{11}}},$$

and $B_{11} = 0$ due to the symmetry at mid-surface. The eight constants C_i are determined by the four natural boundary conditions at the free edge deduced from Equation (20) with $P^*_{(a)} = 0$, namely,

$$0 = A_{11}u_{1,1}^{0*}(L) - \tilde{K}\phi_{1,1}(L), \qquad\qquad 0 = -D_{11}w_{,111}(L) + \tilde{T}\phi_{1,11}(L) - q,$$

$$0 = -D_{11}w_{,11}(L) + \tilde{T}\phi_{1,1}(L), \qquad\qquad 0 = -\tilde{K}u_{1,1}^{0*}(L) + \tilde{T}w_{,11}(L) - \tilde{S}\phi_{1,1}(L),$$
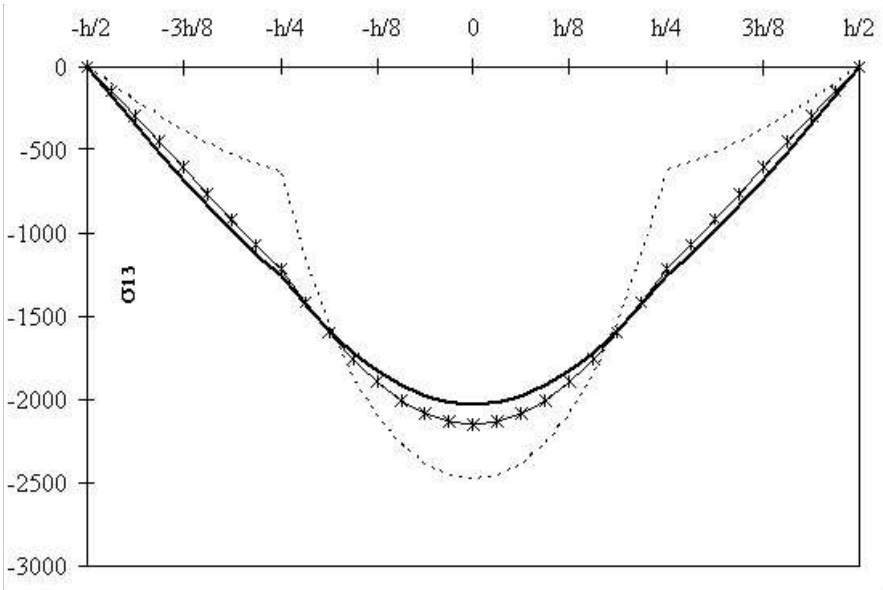
Figure 7. Variation of the stress σ_{13} through the thickness for $x_1 = L/2$ at $x_3 = 0$ for Section 3.3. Abaqus (dashed line plot), Sine (solid line), and Present (dashes and crosses).
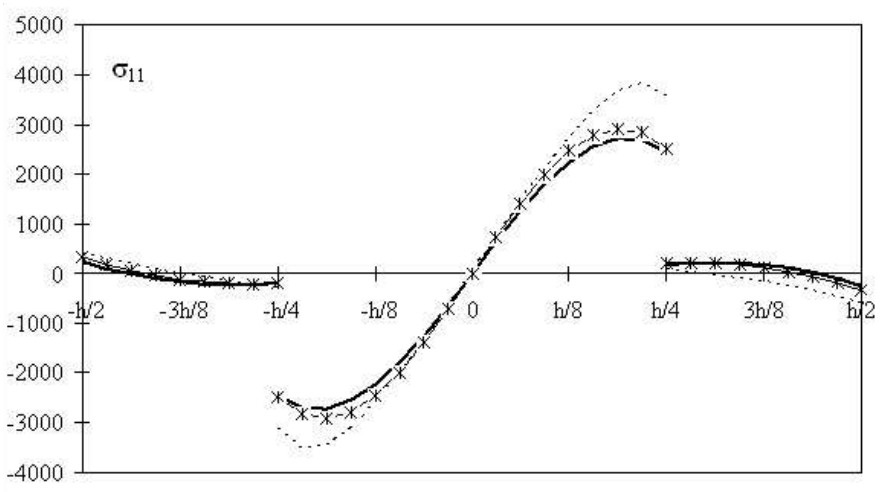
Figure 8. Variation of the stress σ_{11} through the thickness for $x_1 = 3L/4$ for Section 3.3. Abaqus (dashed line plot), Sine (solid line), and Present (dashes and crosses).
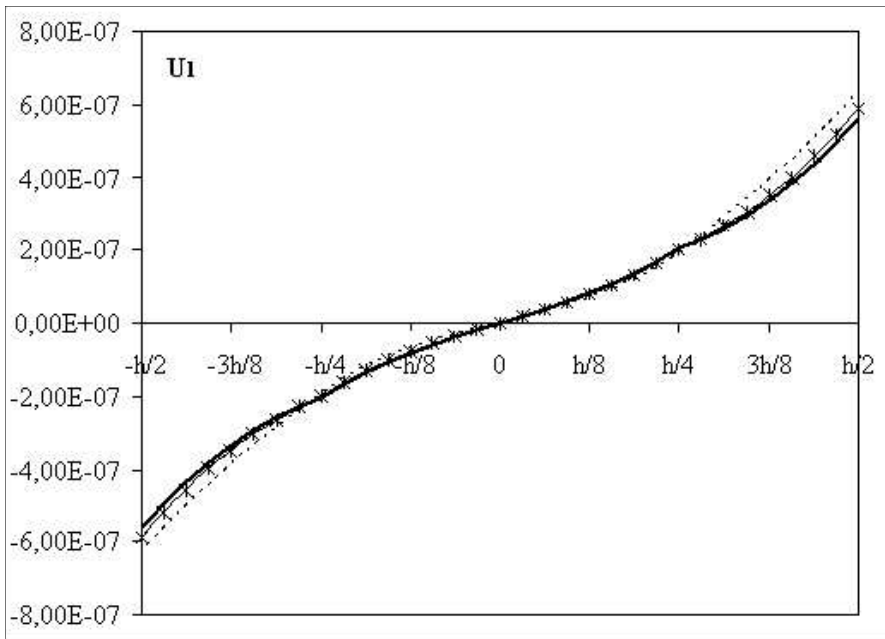
Figure 9. Variation of the displacement U_1 through the thickness for $x_1 = L/4$ for Section 3.3. Abaqus (dashed line plot), Sine (solid line), and Present (dashes and crosses).
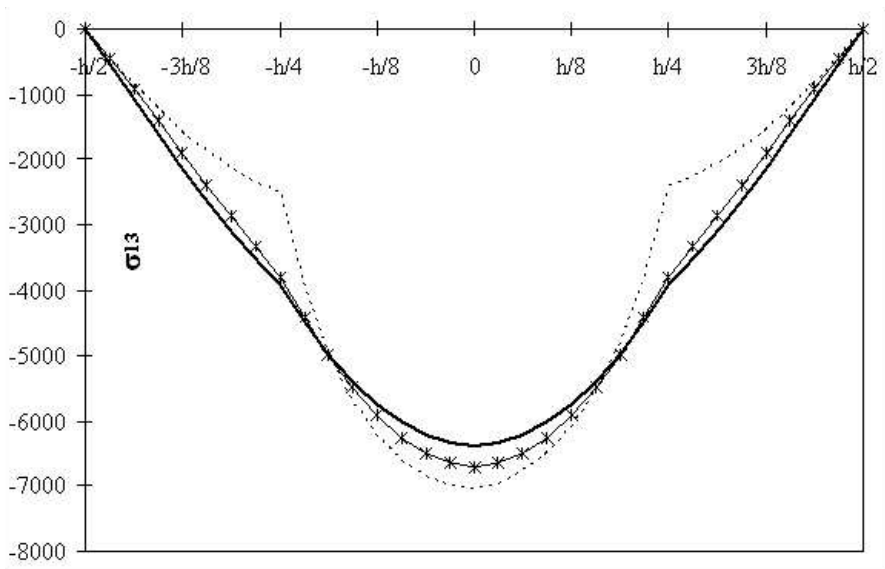
Figure 10. Variation of the stress σ_{13} through the thickness for $x_1 = L/4$ for Section 3.4. Abaqus (dashed line plot), Sine (solid line), and Present (dashes and crosses).

Model	$U_3(L)$	$U_1(L/2, h/2)$	$\sigma_{13}(L/4, 0)$ (Interface)	$\sigma_{11}(L/2, -h/4)$ (Interface)
	[m]	[m]	[Pa]	[Pa]
Present (error)	-1.67021×10^{-5} (0.1%)	2.87160×10^{-6} (8.8%)	-6699.43 (4.7%)	-62969.5 (-1.4%)
Sine (error)	-1.65722×10^{-5} (0.8%)	2.81698×10^{-6} (10.5%)	-6372.07 (9.3%)	-62969.5 (-1.4%)
Abaqus	-1.67110×10^{-5}	3.14800×10^{-6}	-7027.00	-62091.0

Table 3. Bending of a clamped/free thick beam under concentrated load.

along with the four kinematic boundary conditions at the clamped edge:

$$u_1^0(0) = 0,$$
$$w(0) = 0,$$
$$w_{,1}(0) = 0,$$
$$\phi_1(0) = 0.$$

The numerical results presented in Table 3 obtained $q = -10000\,\text{N}$ using the present model for the same beam as in Section 3.3 except that loading is now concentrated at the free end of the beam, our reference still being the Karama et al. [1998] results, show that the present model still has very good results compared to the sine model except with regard to membrane stress (σ_{11}) where no difference was found.

4. Conclusion

Continuity of displacement and transverse shear stresses at layer interfaces and the boundary conditions for a laminated composite are fully satisfied by this present new multilayered structure exponential with the help of the Heaviside step function (Figures 2–10). For the new proposed model the results are compared to the existing model (like the sine model by Touratier [1991]) and by the finite element method by Abaqus [Karama et al. 1998]. Results show that the new proposed exponential model presents a better approximation than the sine [Karama et al. 1998] model when compared to results obtained using finite element analyses, with certain exceptions (Tables 1–3). Specifically results are very favorable at layer interfaces.

The new model is also simple in so far as no correction factor is used, contrary to the other higher order models.

In the case of static analysis the numerical results for the bending deformation under different types of loading and boundary conditions on a thick beam (Figures 2–10) showed that the present model is always closer to the finite element analysis by Abaqus [Karama et al. 1998].

On the whole, we can conclude that the present exponential model is more accurate than other existing analytical models for multilayered structures when compared to finite element analysis.

Appendix A. Virtual power of the acceleration quantities

We have

$$\ddot{U}_1 = \ddot{u}_1^o - x_3\ddot{w}_{,1} + h_1\ddot{\phi}_1, \qquad \ddot{U}_3 = \ddot{w},$$
$$U_1^* = u_1^{0*} - x_3 w_{,1}^* + h_1\phi_1^*, \qquad U_3^* = w^*.$$

So Equation (5) becomes

$$P_{(a)}^* = \int_\Omega \rho(U_1^*\ddot{U}_1 + U_3^*\ddot{U}_3)d\Omega$$

$$= \int_\Omega \rho\big[u_1^{0*}\ddot{u}_1 + (\ddot{u}_3 + x_3\ddot{u}_{1,1})w^* + h_1(x_3)\phi_1^*\ddot{u}_1\big]d\Omega - \int_\Gamma \rho x_3 w^*\ddot{u}_1 d\Gamma$$

$$= \int_\Omega \rho\Big[\big(\ddot{u}_1^o - x_3\ddot{w}_{,1} + h_1(x_3)\ddot{\phi}_1\big)u_1^{0*} + \big(\ddot{w} + x_3(\ddot{u}_{1,1}^o - x_3\ddot{w}_{,11} + h_1(x_3)\ddot{\phi}_{1,1})\big)w^*$$

$$+ h_1(x_3)\big(\ddot{u}_1^o - x_3\ddot{w}_{,1} + h_1(x_3)\ddot{\phi}_1\big)\phi_1^*\Big]d\Omega$$

$$- \int_\Gamma \rho x_3\big(\ddot{u}_1^o - x_3\ddot{w}_{,1} + h_1(x_3)\ddot{\phi}_1\big)w^* d\Gamma,$$

where in the second line we integrated by parts.

Then,

$$P_{(a)}^* = \int_0^L \Bigg[u_1^{0*}\int_{-h/2}^{h/2}\Big(\rho\ddot{u}_1^o - \rho x_3\ddot{w}_{,1} + \rho h_1(x_3)\ddot{\phi}_1\Big)dx_3$$

$$+ w^*\int_{-h/2}^{h/2}\Big(\rho\ddot{w} + \rho x_3\ddot{u}_{1,1}^0 + \rho x_3^2\ddot{w}_{,11} + \rho x_3 h_1(x_3)\ddot{\phi}_{1,1}\Big)dx_3$$

$$+ \phi_1^*\int_{-h/2}^{h/2}\Big(\rho h_1(x_3)\ddot{u}_1^0 - \rho x_3 h_1(x_3)\ddot{w}_{,1} + \rho h_1^2(x_3)\ddot{\phi}_1\Big)dx_3\Bigg]dx_1$$

$$+ w^*\int_{-h/2}^{h/2}\Big(-\rho x_3\ddot{u}_1^o + \rho x_3^2\ddot{w}_{,1} - \rho x_3 h_1(x_3)\ddot{\phi}_1 L\Big)dx_3$$

$$= \int_0^L \big(\Gamma^{(u)}u_1^{0*} + \Gamma^{(w)}w^* + \Gamma^{(\phi)}\phi_1^*\big)dx_1 + \bar{\Gamma}^{(w)}w^*,$$

where the last line comes from using the relations (6).

Appendix B. Virtual power of the internal work

By relation (9), virtual power of the internal work (8) becomes

$$
\begin{aligned}
P_{(i)}^* &= -\int_{\Omega}\Big[\big(u_{1,1}^{0*}-x_3 w_{,11}^*+h_1(x_3)\phi_{1,1}^*\big)\sigma_{11}+2\big(\tfrac{1}{2}h_{1,3}(x_3)\phi_1^*\big)\sigma_{13}\Big]d\Omega \\
&= -\int_{\Omega}\Big[-\sigma_{11,1}u_1^{0*}-x_3\sigma_{11,11}w^*-h_1(x_3)\sigma_{11,1}\phi_1^*+h_{1,3}(x_3)\sigma_{13}\phi_1^*\Big]d\Omega \\
&\qquad\qquad -\int_{\Gamma}\Big[\sigma_{11}u_1^{0*}-x_3\sigma_{11}w_{,1}^*+x_3\sigma_{11,1}w^*+h_1(x_3)\sigma_{11}\phi_1^*\Big]d\Gamma \\
&= \int_0^L\Big[u_1^{0*}\int_{-h/2}^{h/2}\sigma_{11,1}dx_3+w^*\int_{-h/2}^{h/2}x_3\sigma_{11,11}dx_3+\phi_1^*\int_{-h/2}^{h/2}\big(h_1(x_3)\sigma_{11,1}-h_{1,3}(x_3)\sigma_{13}\big)dx_3\Big]dx_1 \\
&\qquad -u_1^{0*}\int_{-h/2}^{h/2}\sigma_{11}dx_3+w_{,1}^*\int_{-h/2}^{h/2}x_3\sigma_{11}dx_3-w^*\int_{-h/2}^{h/2}x_3\sigma_{11,1}dx_3-\phi_1^*\int_{-h/2}^{h/2}h_1(x_3)\sigma_{11}dx_3,
\end{aligned}
$$

where in the second line we integrated by parts.

Using relations (10), we obtain

$$
P_{(i)}^* = \int_0^L\big(N_{11,1}u_1^{0*}+M_{11,11}w^*+(P_{11,1}-P_{13})\phi_1^*\big)dx_1-N_{11}u_1^{0*}-M_{11,1}w^*+M_{11}w_{,1}^*-P_{11}\phi_1^*.
$$

Appendix C. Virtual power of the external loading

By relations (13), virtual power of external loading (12) becomes

$$
\begin{aligned}
P_{(e)}^* &= \int_{\Omega}\begin{bmatrix}U_1^* & 0 & U_3^*\end{bmatrix}\cdot\begin{bmatrix}f_1\\f_2\\f_3\end{bmatrix}d\Omega+\int_{\Gamma}\begin{bmatrix}U_1^* & 0 & U_3^*\end{bmatrix}\cdot\begin{bmatrix}F_1\\F_2\\F_3\end{bmatrix}d\Gamma \\
&= \int_{\Omega}\big(f_1 U_1^*+f_3 U_3^*\big)d\Omega+\int_{\Gamma}\big(F_1 U_1^*+F_3 U_3^*\big)d\Gamma \\
&= \int_{\Omega}\big(f_1 u_1^{0*}-f_1 x_3 w_{,1}^*+h_1(x_3)f_1\phi_1^*+f_3 w^*\big)d\Omega+\int_{\Gamma}\big(F_1 u_1^{0*}-F_1 x_3 w_{,1}^*+h_1(x_3)F_1\phi_1^*+F_3 w^*\big)d\Gamma \\
&= \int_0^L\Big[u_1^{0*}\int_{-h/2}^{h/2}f_1 dx_3+w^*\int_{-h/2}^{h/2}\big(f_3+x_3 f_{1,1}\big)dx_3+\phi_1^*\int_{-h/2}^{h/2}h_1(x_3)f_1 dx_3\Big]dx_1 \\
&\qquad +u_1^{0*}\int_{-h/2}^{h/2}F_1 dx_3+w^*\int_{-h/2}^{h/2}\big(F_3-x_3 f_1\big)dx_3+\phi_1^*\int_{-h/2}^{h/2}h_1(x_3)F_1 dx_3-w_{,1}^*\int_{-h/2}^{h/2}x_3 F_1 dx_3 \\
&= \int_0^L\big(\overline{n}_1 u_1^{0*}+(\overline{n}_3+\overline{m}_{1,1})w^*+\overline{p}_1\phi_1^*\big)dx_1+\overline{N}_1 u_1^{0*}(\overline{N}_3-\overline{m}_1)w^*-\overline{M}_1 w_{,1}^*+\overline{P}_1\phi_1^*,
\end{aligned}
$$

where the last line utilizes relation (13).

References

[Ambartsumian 1958] S. A. Ambartsumian, "On theory of bending plates", *Izv. Otd. Tech. Nauk. AN SSSR* **5** (1958), 69–77.

[Beakou 1991] A. Beakou, *Homogénéisation et modélisation des coques composites multicouches*, PhD Thesis, ENSAM, Paris, 1991.

[Di Sciuva 1987] M. Di Sciuva, "An improved shear deformation theory for moderately thick multi-layered anisotropic shells and plates", *J. Appl. Mech.* (*Trans. ASME*) **54** (1987), 589–596.

[Di Sciuva 1993] M. Di Sciuva, "A general quadrilateral multilayered plate element with continuous interlaminar stresses", *Comput. Struct.* **47**:1 (1993), 91–105.

[He 1994] L. H. He, "A linear theory of laminated shells accounting for continuity of displacements and transverse shear stresses at layer interfaces", *Int. J. Solids Struct.* **31**:5 (1994), 613–627.

[Idlbi 1995] A. Idlbi, *Comparaison de théories de plaque et estimation de la qualité des solution dans la zone bord*, PhD Thesis, ENSAM, Paris, 1995.

[Kaczkowski 1968] Z. Kaczkowski, *Plates-statistical calculations*, Arkady, Warsaw, 1968.

[Karama et al. 1998] M. Karama, B. Abouharb, S. Mistou, and S. Caperaa, "Bending, buckling and free vibration of laminated composite with a transverse shear stress continuity model", *Compos. B:Eng.* **29**:3 (1998), 223–234.

[Kirchhoff 1850] G. J. Kirchhoff, "Über das Gleichgewicht und die Bewegung einer elastischen Schreitbe", *Reine Angew Math* **40** (1850), 51–58.

[Levinson 1980] M. Levinson, "An accurate simple theory of the statics and dynamics of elastic plates", *Mech. Res. Commun.* **7**:6 (1980), 343–350.

[Love 1934] A. E. H. Love, *A treatise on the mathematical theory of elasticity*, 4 ed., Cambridge University Press, 1934.

[Mindlin 1951] R. D. Mindlin, "Influence of rotary inertia and shear on flexural motions of isotropic elastic plates", *J. Appl. Mech.* (*Trans. ASME*) **18** (1951), 31–38.

[Murthy 1981] M. V. V. Murthy, "An improved transverse shear deformation theory for laminated anisotropic plates", NASA Technical Paper, 1981, Available at http://ntrs.nasa.gov/archive/nasa/casi.ntrs.nasa.gov/19820003615_1982003615% .pdf.

[Ossadzow et al. 1995] C. Ossadzow, P. Muller, and M. Touratier, *Une théorie générale des coques composites multicouches*, vol. 1, Deuxième Colloque National en Calcul des Structures, Hermes, 1995.

[Pagano 1970] N. J. Pagano, "Exact solution for rectangular bi-directional composites and sandwich plates", *J. Compos. Mater.* **4** (1970), 20–34.

[Panc 1975] V. Panc, *Theories of elastic plates*, Academia, Prague, 1975.

[Reddy 1984] J. N. Reddy, "A simple high-order theory of laminated composite plate", *J. App. Mech.* (*Trans. ASME*) **51** (1984), 745–752.

[Reissner 1945] E. Reissner, "Reflection on the theory of elastic plates", *J. Appl. Mech.* (*Trans. ASME*) **38** (1945), 1453–1464.

[Reissner 1975] E. Reissner, "On transverse bending of plates, including the effect of transverse shear deformation", *Int. J. Solids Struct.* **11**:5 (1975), 569–573.

[Touratier 1991] M. Touratier, "An efficient standard plate theory", *Int. J. Eng. Sci.* **29**:8 (1991), 901–916.

[Touratier 1992] M. Touratier, "A generalization of shear deformation theories for axisymmetric multilayered shells", *Int. J. Solids Struct.* **29**:11 (1992), 1379–1399.

[Widera and Logan 1980] G. E. O. Widera and D. L. Logan, "Refined theories for non-homogeneous anisotropic cylindrical shells, I and II", *J. Eng. Mech. Div. ASCE* **EM6** (1980), 1053–1090.

M. KARAMA: moussa@enit.fr
École Nationale d'Ingénieurs de Tarbes, 47 av. Azereix BP1629, 65016 Tarbes, France

K. S. AFAQ: kamran@enit.fr
École Nationale d'Ingénieurs de Tarbes, 47 av. Azereix BP1629, 65016 Tarbes, France

S. MISTOU: mistou@enit.fr
École Nationale d'Ingénieurs de Tarbes, 47 av. Azereix BP1629, 65016 Tarbes, France